Impacts of Snow Initialization on Subseasonal Forecasts of Surface Air Temperature for the Cold Season

JEE-HOON JEONG,* HANS W. LINDERHOLM,+ SUNG-HO WOO,# CHRIS FOLLAND,@ BAEK-MIN KIM,& SEONG-JOONG KIM,& AND DELIANG CHEN+

* *Faculty of Earth Systems and Environmental Sciences, Chonnam National University, Gwangju, South Korea*
+ *Department of Earth Sciences, University of Gothenburg, Gothenburg, Sweden*
# *Korea Institute of Ocean Science and Technology, Ansan, and School of Earth and Environmental Sciences, Seoul National University, Seoul, South Korea*
@ *Department of Earth Sciences, University of Gothenburg, Gothenburg, Sweden, and Met Office Hadley Centre, Exeter, United Kingdom*
& *Korea Polar Research Institute, Incheon, South Korea*

(Manuscript received 17 March 2012, in final form 15 September 2012)

ABSTRACT

The present study examines the impacts of snow initialization on surface air temperature by a number of ensemble seasonal predictability experiments using the NCAR Community Atmosphere Model version 3 (CAM3) AGCM with and without snow initialization. The study attempts to isolate snow signals on surface air temperature. In this preliminary study, any effects of variations in sea ice extent are ignored and do not explicitly identify possible impacts on atmospheric circulation. The Canadian Meteorological Center (CMC) daily snow depth analysis was used in defining initial snow states, where anomaly rescaling was applied in order to account for the systematic bias of the CAM3 snow depth with respect to the CMC analysis. Two suites of seasonal (3 months long) ensemble hindcasts starting at each month in the colder part of the year (September–April) with and without the snow initialization were performed for 12 recent years (1999–2010), and the predictability skill of surface air temperature was estimated. Results show that considerable potential predictability increases up to 2 months ahead can be attained using snow initialization. Relatively large increases are found over East Asia, western Russia, and western Canada in the later part of this period. It is suggested that the predictability increases are sensitive to the strength of snow–albedo feedback determined by given local climate conditions; large gains tend to exist over the regions of strong snow–albedo feedback. Implications of these results for seasonal predictability over the extratropical Northern Hemisphere and future direction for this research are discussed.

1. Introduction

The prediction of weather and climate for more than 2 weeks ahead relies largely on memories from slowly varying processes in the ocean, sea ice, and the land surface. In particular, present-day dynamical seasonal prediction greatly benefits from the skillful prediction of tropical and extratropical sea surface temperature (SSTs), mainly but not exclusively based on advances in physical understanding of the El Niño–Southern Oscillation (ENSO) (Shukla et al. 2000; Wang et al. 2008). However, the major contribution of such SST prediction to seasonal forecasts is currently largely confined to the tropics and subtropics though an ENSO signal in higher latitudes has been identified in later winter (Ineson and Scaife 2009). Although tropical SSTs do have considerable remote impacts on extratropical climate (Kumar et al. 2005; Trenberth et al. 1998), overall seasonal predictability by general circulation models (GCMs) is still poor in extratropics and continental interiors where the influences of SST forcings are indirect and insignificant (Wang et al. 2008).

Recently there has been a growing interest in other, slowly varying, physical processes in the climate system, which can provide conventional seasonal prediction with additional sources of skill especially on extratropical continents. Possible contributions to subseasonal and seasonal predictability from land surface conditions (e.g., Koster et al. 2011, 2010b), stratospheric circulation

Corresponding author address: Baek-Min Kim, Korea Polar Research Institute, 7-50 Songdo-dong, Yeonsu-gu, Incheon, South Korea.
E-mail: bmkim@kopri.re.kr

DOI: 10.1175/JCLI-D-12-00159.1

(Ambaum and Hoskins 2002; Baldwin et al. 2003; Folland et al. 2011; Ineson et al. 2011), and sea ice extents (Alexander et al. 2004; Deser et al. 2007, 2004; Honda et al. 2009) have been identified. Among them, contributions of soil moisture conditions to subseasonal and seasonal prediction have recently been quite extensively studied. According to multimodel retrospective forecast experiments with realistically initialized soil moisture from the Global Land–Atmosphere Coupling Experiment (GLACE2) project, initial soil-wetness conditions provide significant increase in the skill of air temperature predictions with up to 2 months lead time during summer, in particular, over semiarid continental interiors where the land–atmosphere interaction is strong (Koster et al. 2011, 2010b).

During the winter half year, snow cover or depth has been regarded as a candidate predictor for climate over continental interiors in the middle to high latitudes (e.g., Cohen and Fletcher 2007; Cohen and Jones 2011; Orsolini and Kvamstø 2009). This results from the physical properties of snow: high reflectance to shortwave radiation (high albedo), strong emissivity, and low thermal conductivity, which lead to significant impacts on local weather and climate. For instance, above-normal snow tends to cool the near-surface air by reflecting more incoming solar radiation and emitting longwave radiation more efficiently but keeps underlying soil temperature higher. During snowmelt, the melting snowpack absorbs large amounts of latent heat and releases water to the soil, affecting the land surface energy budget and hydrological cycle and leading to local cooling. Not surprisingly, the important role of snow-related feedbacks on climate model simulations has previously been recognized (e.g., Cohen and Rind 1991; Yeh et al. 1983) with an early attempt at assessing its influence on seasonal predictability (Saunders et al. 2003). Moreover, the influence of snow on local climate variability is known to be much larger than that of SST over many parts of the extratropical land (Kumar and Yang 2003). In addition to local impacts on near-surface climate, it has been suggested that large-scale snow cover change could invoke remote and delayed influences through altering the large-scale atmospheric circulation. For instance, the impacts of fall Eurasian snow cover on hemispheric circulation modes, like the northern annular mode or the North Atlantic Oscillation, have been found in both observations and climate model experiments (Cohen et al. 2007; Fletcher et al. 2009a; Saito et al. 2001). The rate of Eurasian snow cover increase during October was found to be highly correlated to the wintertime Arctic Oscillation (Cohen and Jones 2011). In addition, a marked impact of snow cover changes and associated feedback effects has been identified on long-term future climate projections by the Intergovernmental Panel on Climate Change (IPCC) Fourth Assessment Report (AR4) climate models (Fletcher et al. 2009b; Jeong et al. 2011; Winton 2006a,b).

Despite its apparent importance, the utilization of snow information for extended-range and seasonal forecasts by GCMs is limited. In addition to difficulties in accurate physical parameterization of snow and the associated feedbacks, the lack of snow observations has been a major obstacle for practical applications. A few instrumental records are available for regions in the high latitudes (Armstrong 2001; Brown et al. 2003), but these are in general insufficient to perform multiyear global model experiments, in terms of both spatial coverage and temporal availability. Remote sensing by satellite enables snow cover concentration and areal extent to be retrieved globally and such data has been utilized in investigations of the impact of large-scale snow anomalies on climate (Fletcher et al. 2009a; Orsolini and Kvamstø 2009). However, rather than snow cover extent, depth information is preferable for climate prediction as it contains a better source of memory for influencing subsequent climate. Besides the fractional cover, physical variables like snow mass or snow water equivalent can be estimated from the depth information. There are empirical techniques to estimate snow mass from snow cover, but these two variables are not necessarily well related; thus, on a continental scale there is almost no association between them (Ge and Gong 2008). An alternative approach is to derive snow states from offline calculations using a land surface model indirectly, driven by observed surface meteorological forcings. This approach has been utilized for springtime predictions of temperature (Peings et al. 2010) and streamflow (Koster et al. 2010a).

In the present study, we construct snow state parameters for the initial condition of climate model hindcasts using an observation-based, daily snow depth analysis over the Northern Hemisphere for the period 1999–2010. By performing retrospective ensemble seasonal prediction experiments, the impacts of initialized snow states on predictability are examined. Details of the modeling system, initialization procedure, and experiments are described in section 2; the analysis and discussions of potential and practical predictability skills are presented in section 3; and a summary and discussion are presented in section 4.

2. Experiments

a. Climate model

This study utilized the Community Atmosphere Model version 3 (CAM3), an atmospheric general circulation

model developed by the National Center for Atmospheric Research (Collins et al. 2004). To save time and resource required for the model runs, in this preliminary study, we chose to use an atmospheric GCM (AGCM) for hindcasts rather than a coupled ocean–atmosphere GCM. We updated the cloud scheme in the CAM3 with the freeze-dry modification, which reduces an excessive bias in cloud cover in the Arctic (Vavrus and Waliser 2008). The chosen horizontal resolution of the CAM3 experiments is 2° longitude by 2.5° latitude (for both atmosphere and land), with 26 hybrid-sigma vertical levels encompassing the surface to the midstratosphere (1 hPa). Incorporated into CAM3 is the Community Land Model version 3 (CLM3; Oleson et al. 2004), which simulates various geophysical and hydrological processes at the land surface and its subsurface layers. The CLM3 simulates snow states with multiple snow layers (maximum of five layers) of different thickness and age parameterizing new snowfall accumulation, compaction, melting, and freezing of snow layers. Therefore, synchronous land–atmosphere coupling enables the CAM3–CLM3 to simulate snow-related feedback processes.

b. Snow initialization

The Canadian Meteorological Center (CMC) daily snow depth analysis data (Brasnett 1999; Brown and Bruce 2010) were used to initialize snow states in the CAM3 experiments. The CMC data, which are a synthesis of surface synoptic observations and aviation reports, provide monthly averages and monthly climatologies of snow depth and estimated snow water equivalent. They are available since 12 March 1998 and cover the entire Northern Hemisphere with a horizontal resolution of 24 km by 24 km. Prior to model initialization, data from the original horizontal resolution were converted to the model grid (2° longitude × 2.5° latitude) by local area averaging.

In Figs. 1 and 2, the long-term average snow depth and estimated snow cover from the CMC are compared to these variables derived from other observational and reanalysis datasets and the AMIP-type CAM3 simulations. The CMC data shows higher snow depths compared to the European Centre for Medium-Range Weather Forecasts (ECMWF) Interim Re-Analysis (ERA-Interim; Dee and Uppala 2009; Dee et al. 2011) throughout the whole winter period over middle to high latitudes (Fig. 1). Compared to CAM3, however, the CMC data tend to exhibit lower snow depths over most of the high latitudes and pan-Arctic regions, except for higher depths over the Tibetan Plateau and Eastern Europe. Figure 2 compares with the long-term mean snow cover estimated from the CMC data, the satellite-based snow cover data produced by the National Oceanic and Atmospheric Administration (NOAA) (Robinson et al. 1993), and the CAM3 simulation. The CMC data show lower fractional snow cover over the high latitudes but slightly higher cover over the high latitudes compared to NOAA data. The CMC mean snow cover and snow line patterns in the midlatitudes and its seasonal march overall agree quite well with the CAM3 simulation, but notable differences are found over many high-latitude regions and the Tibetan plateau. As expected from the mean snow depth comparison, the CMC snow cover is slightly lower over most high latitudes.

This systematic bias of CAM3 simulation compared with CMC data suggests that the CMC data need some calibration in order to be directly applied to the CAM3 input. Besides the bias in the mean, the CAM3 snow depth exhibits generally weaker interannual variability (lower standard deviation) compared to the CMC (figure not shown), a common bias found in most of the current GCMs (Hardiman et al. 2008). If the CMC data are used directly in the model simulations without calibration, such biases may result in poor GCM forecasts. For instance, relatively large amounts of snow in the CMC analysis in high latitudes could mean relatively small amount of snow in terms of the CAM3 average. Alternatively, a small depth change in the CMC analysis could mean huge depth change in the CAM3 as model variability is much smaller than that of the CMC analysis. Therefore, biases in the initial conditions often lead to a serious climate drift; thus, inappropriately initialized snow quickly converges to the model default state or creates an artificial shock in the model system, rather than providing a useful memory for the seasonal forecast. To prevent this happening, we applied a standard normal deviate scaling to the CMC snow depth analysis. Based on long-term statistics (mean and standard deviation) for model and observation, the scaled snow depth for the model initial condition (F_m) can be estimated from following relationship:

$$\frac{F_o - \overline{F}_o}{\sigma(F_o)} = \frac{F_m - \overline{F}_m}{\sigma(F_m)},$$

where the overbar indicates long-term mean and σ indicates standard deviation of the variable. The mean and standard deviation of the model were estimated from the preexisting AMIP-type 16-member ensemble simulations, forced with observed SSTs and sea ice concentrations. We call this the rescaled anomaly initialization. Similar approaches have been widely used for observation-based soil-moisture initialization of climate model simulations and shown to be effective (Jeong et al. 2008; Koster et al. 2004, 2011).

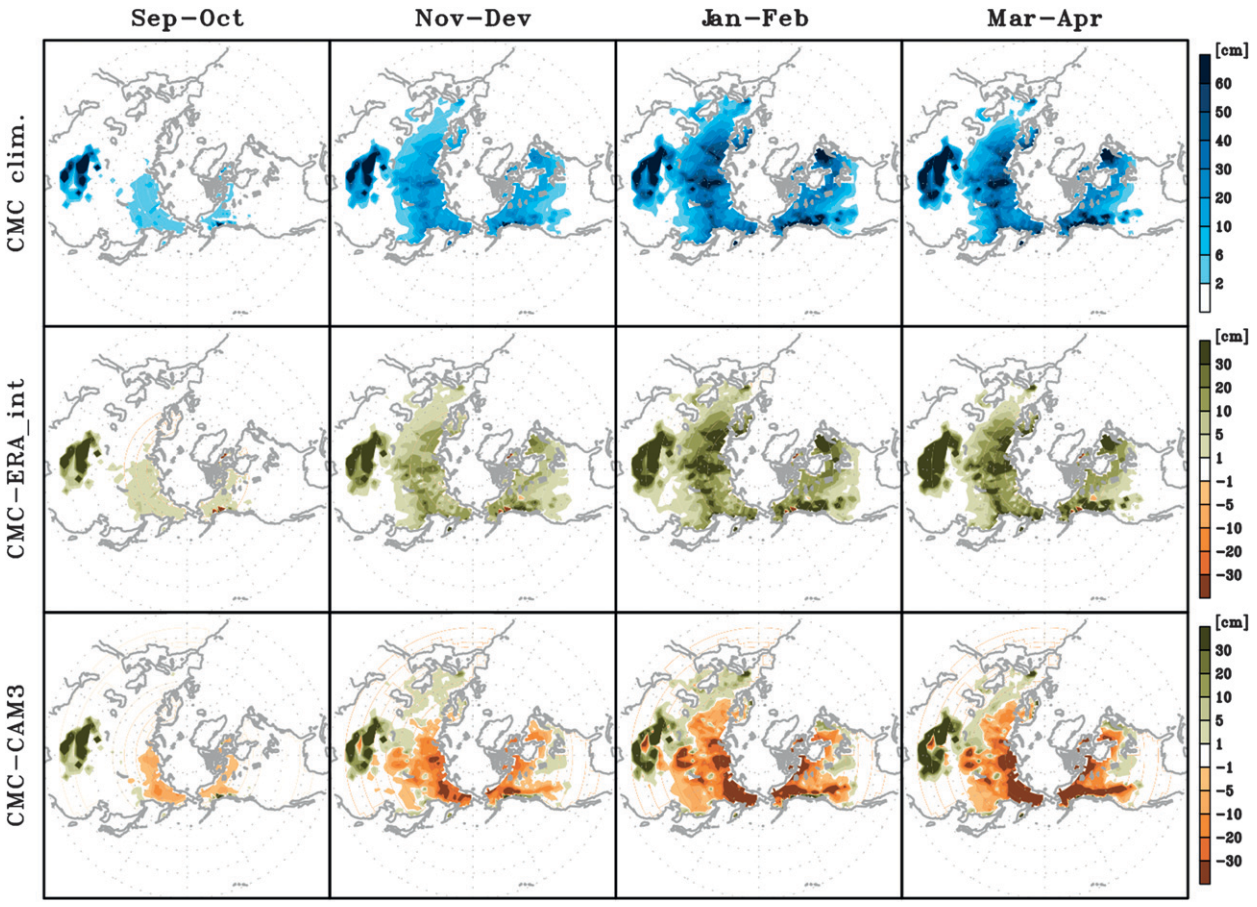

FIG. 1. (top) Long-term means of CMC snow depth for the cold season and their differences from those of (middle) ERA-Interim snow depth and (bottom) AMIP-type CAM3 simulations.

From the rescaled anomaly snow depth data, snow states need to be defined. The total number of snow layers and the thickness of each layer are defined with the rescaled snow depth according to the initialization processes stated in Oleson et al. (2004). This is summarized in Table 1. Here, the age and liquid water content of the newly defined snow layers are set to zero, assuming all the snow layers consist of fresh snow only. A bulk density of snow, 250 kg m^{-3}, is used for snow density of all layers.

Figure 3 shows several examples of the evolution of snow depth simulated by the CAM3 with and without snow initialization (S1 and S2, respectively; details are given in the next section). For the selected points in central Russia and Canada, initialized snow depths seem to be within reasonable range of model variability, and anomalies tend to persist more than a month without a significant drift. We have checked the entire Northern Hemisphere (NH) and found that the rescaled snow depth anomaly method performs well in the model.

c. *Experimental design*

Two suites of retrospective ensemble seasonal prediction experiments are performed with and without snow initialization (S1 and S2, respectively) during the cold season (September–April) for the period 1999–2010. Starting from the first day of each month, 16 member ensemble runs are performed for 3 months. Consequently, the S1 and S2 series each consist of 1536 simulations (8 months $\times$ 12 yr $\times$ 16 ensembles), providing large enough samples to test the impact of snow initialization on predictability.

Initial and boundary conditions for the two series are identical except for the initial snow states. The atmospheric initial conditions are obtained from the National Centers for Environmental Prediction (NCEP)–U.S. Department of Energy (DOE) Atmospheric Model Intercomparison Project II (AMIP-II) reanalysis (Kanamitsu et al. 2002). The 16 initial atmospheric states (wind, temperature, specific humidity, and surface pressure) are sampled at 6-h intervals at times equal or before the

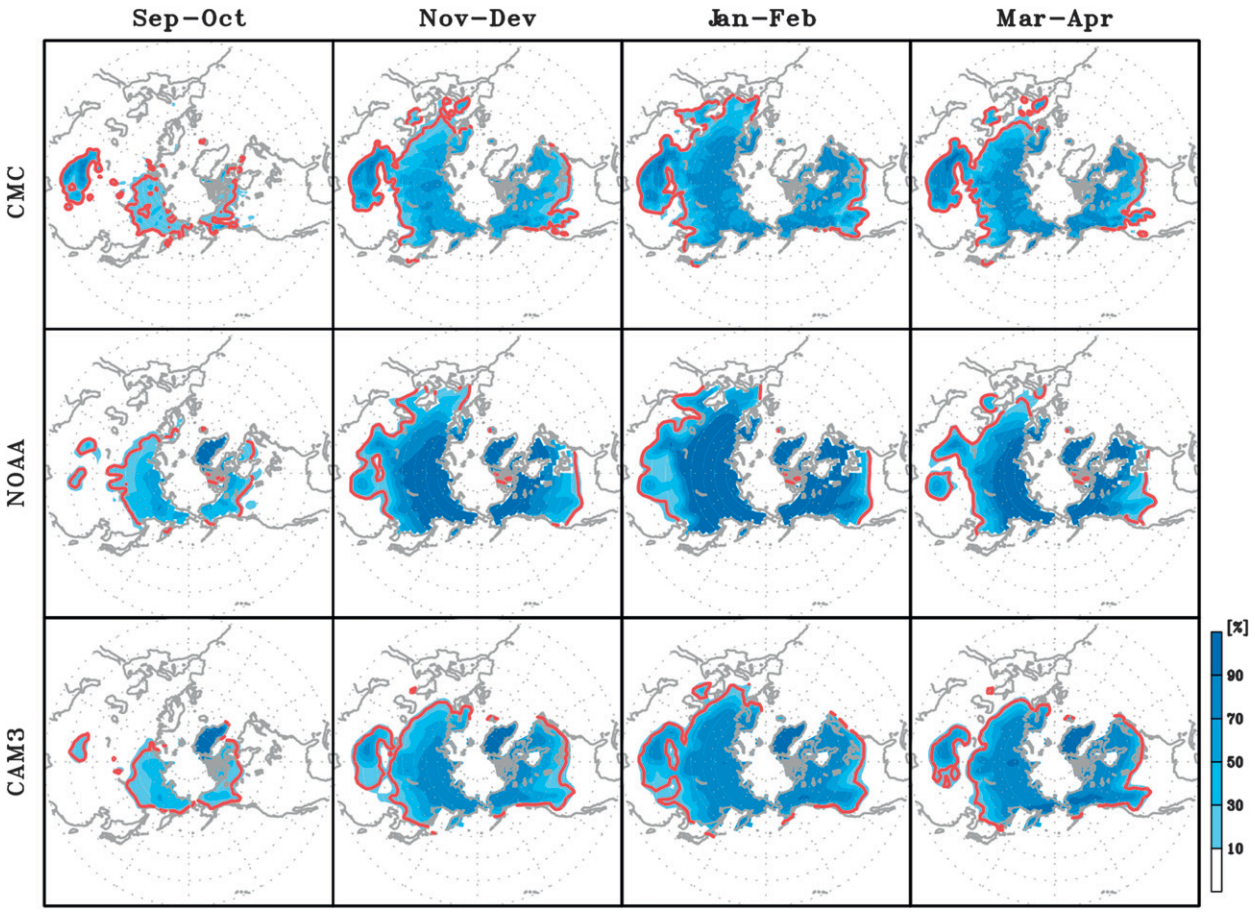

FIG. 2. Long-term means of snow cover from (top) the CMC data, (middle) NOAA/Climate Prediction Center (CPC), and (bottom) AMIP-type CAM3 simulations for the cold season. The red contour line indicates the 15% snow cover fraction. Here, CMC snow cover is transformed from snow depth by an empirical relationship: $SC = D/(10 \times zlnd + D)$, where SC is snow cover (fraction), D is snow depth (m), and, zlnd is the momentum roughness length for soil (0.01 m in the CLM3).

nominal start time of each hindcast. Thus, initial conditions for hindcasts staring at 0000 UTC December 1 are taken from reanalyses at 0000 UTC December 1, 1800 UTC November 30, 1200 UTC November 30, . . . , 0600 UTC November 27. Land surface initial conditions including soil moisture and temperature are taken from the preexisting AMIP-type 16-member ensemble simulations forced with observed SSTs and sea ice concentrations. Like other land surface conditions, the snow states for the S2 series are taken from the AMIP-type simulation, while those for the S1 series are initialized with the rescaled CMC anomaly data. Therefore, there is a smaller spread among initial land surface conditions in S1 compared to that in S2 as the same snow

TABLE 1. The definition of snow layers from the rescaled snow depth.

Depth (D) (m)	Tot No. of layers	Snow layer structure [d_N: depth (m) of the Nth snow layers]
$0.01 \le D \le 0.03$	1	$d_1 = D$
$0.03 < D \le 0.04$	2	$d_2 = D/2, d_1 = d_2$
$0.04 < D \le 0.07$	2	$d_2 = 0.02, d_1 = D - d_2$
$0.07 < D \le 0.12$	3	$d_3 = 0.02, d_2 = (D - 0.02)/2, d_1 = d_2$
$0.12 < D \le 0.18$	3	$d_3 = 0.02, d_2 = 0.05, d_1 = D - d_3 - d_2$
$0.18 < D \le 0.29$	4	$d_4 = 0.02, d_3 = 0.05, d_2 = (D - d_4 - d_3)/2, d_1 = d_2$
$0.29 < D \le 0.41$	4	$d_4 = 0.02, d_3 = 0.05, d_2 = 0.11, d_1 = D - d_4 - d_3 - d_2$
$0.41 < D \le 0.64$	5	$d_5 = 0.02, d_4 = 0.05, d_3 = 0.11, d_2 = (D - d_4 - d_3 - d_2)/2, d_1 = d_2$
$0.64 < D$	5	$d_5 = 0.02, d_4 = 0.05, d_3 = 0.11, d_2 = 0.23, d_1 = D - d_5 - d_4 - d_3 - d_2$

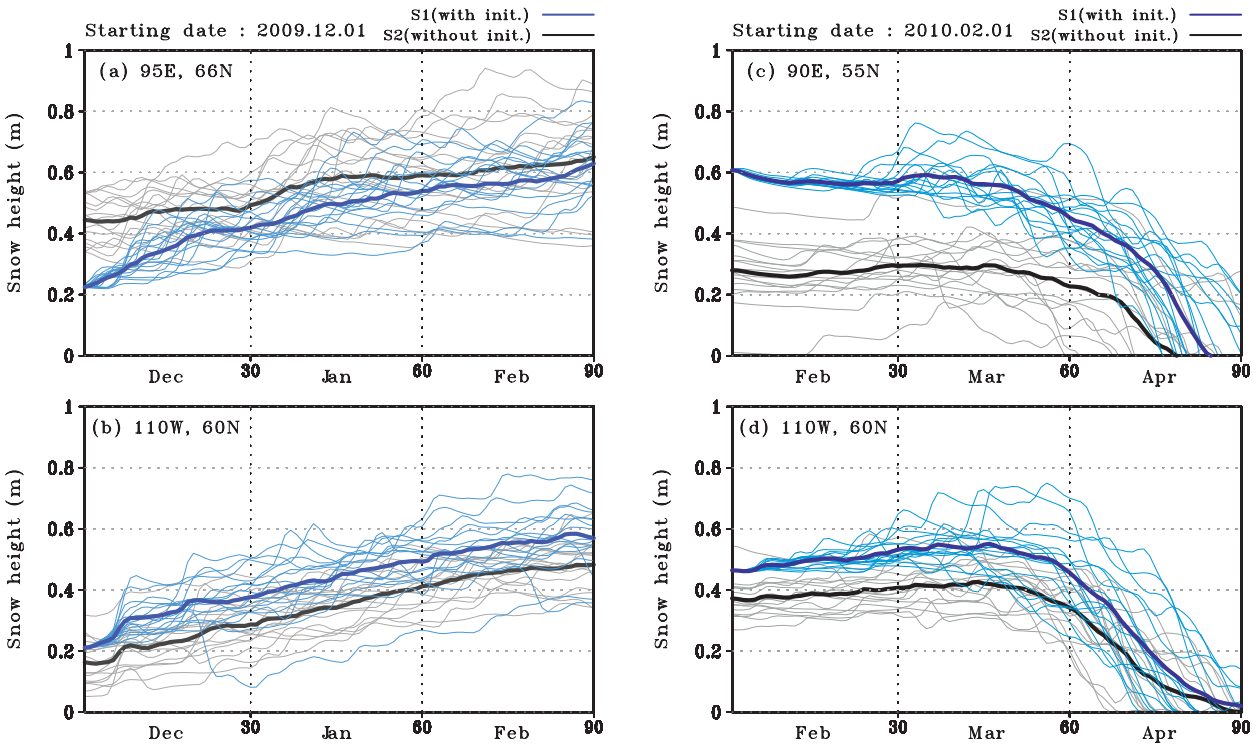

FIG. 3. Simulated snow depth evolution for the ensemble hindcasts started at (left) 1 Dec 2009 and (right) 1 Feb 2010. Blue and black–gray lines indicate simulations with and without snow initialization (S1 and S2), respectively. Thin lines indicate snow depth simulated by 16 ensemble members, and thick lines are ensemble averages: (a) 66°N, 95°E; (b),(d) 60°N, 110°W; and (c) 55°N, 90°E.

condition is used for all ensemble members. The SST boundary condition is prepared by using the conventional anomaly persistence method used with AGCM forecasts. We assume that the anomalous SST observed at the beginning of the hindcast persists through the hindcast period where the initial SST anomaly observed on the starting dates is taken from the NOAA optimum interpolation sea surface temperature (OISST) V2 (Reynolds et al. 2002) weekly data. The anomaly is added via linear interpolation to the climatological mean seasonal cycle of SST for the duration of the hindcast. The sea ice concentration (SIC) is prescribed differently, with only the climatological mean seasonal cycle being used. Climatological mean seasonal cycles of both SST and SIC are taken from the Hadley Centre Global Sea Ice and Sea Surface Temperature dataset (HadISST) (Rayner et al. 2003).

3. Results

a. Potential predictability gain

We first examine the contribution of snow initialization to the potential predictability of near-surface air temperature (SAT). The potential predictability is estimated by the r^2 value suggested by Koster et al. (2004) with a minor modification in averaging r. Here r^2 value (square of the correlation coefficient) measures the degree of agreement between ensemble members as following procedure. Assuming the first ensemble member to be an observation and the ensemble mean of rest of ensemble members (members 2–16) to be a hindcast, r is calculated by linearly regressing hindcast–observation pairs for a chosen month and lead time throughout the 12-yr simulations. This procedure is repeated with the second ensemble member and ensemble mean of rest of ensemble members (members 1 and 3–16). The same process is further repeated with the other remaining ensemble members to get 16 r values. Then we calculate an average of the 16 r values (Fisher's Z transformation is applied to the r values prior to taking an average and then inverse transformation is taken to the average) and square it to yield r^2 value. Therefore, we can assume that higher (lower) r^2, higher (lower) agreement between ensemble members, indicates stronger (weaker) influence of the initialized snow state boundary and thus higher predictability can be possibly obtained from it. In other words, the resulting r^2 values represent the upper limit of predictability, which can be gained by the modeling system with prescribed boundary and initial conditions.

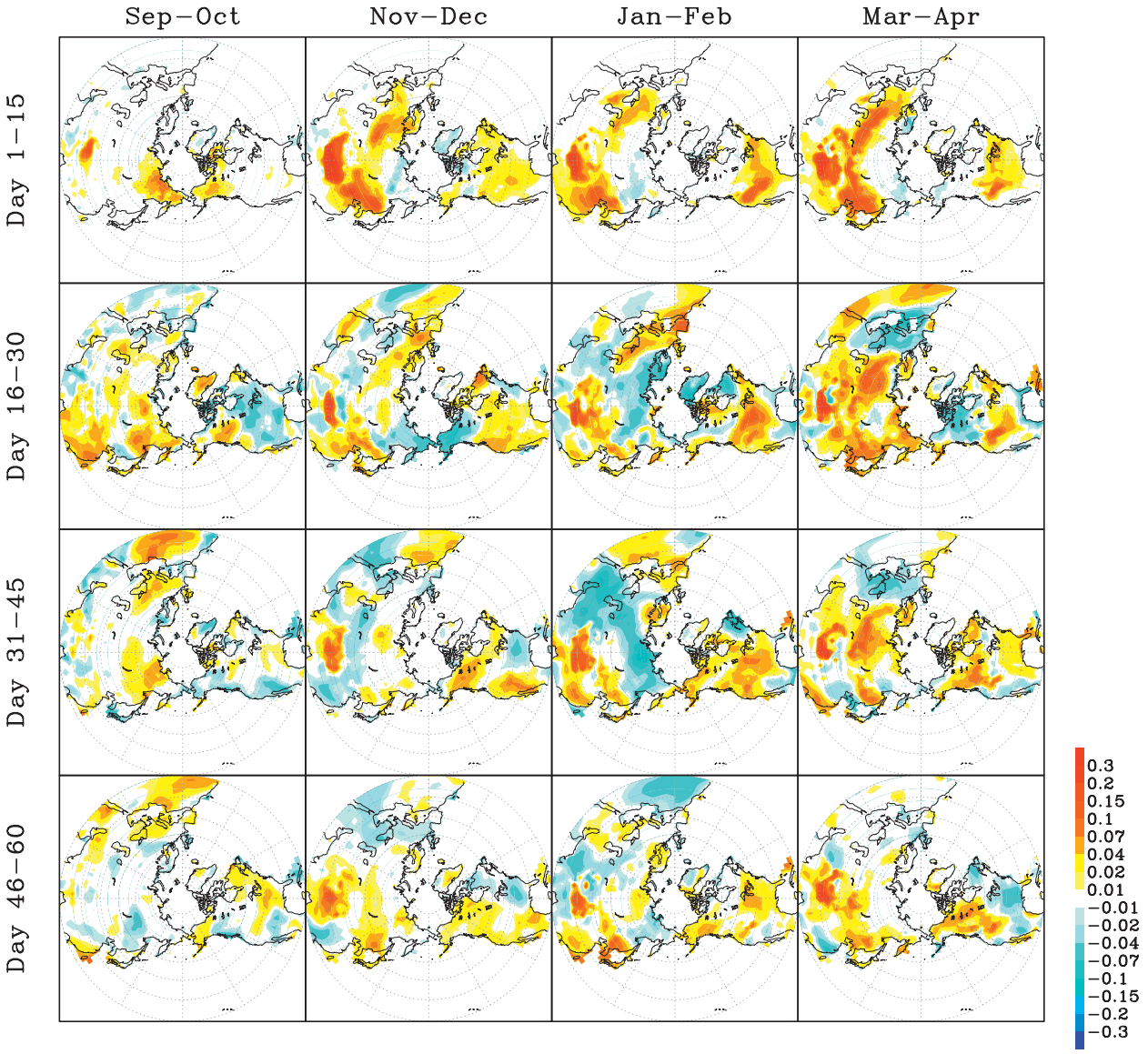

FIG. 4. Change in potential predictability (r^2; see text for details) of SAT hindcast using the snow depth initialization (S1 − S2): (left to right) Sep–Oct to Mar–Apr and (top to bottom) day 1–15 to 46–60.

The potential predictability (r^2) for S1 and S2 is calculated separately and the difference represented in Fig. 4. Because all other conditions but snow condition were identical for S1 and S2, we may assume the difference as an impact of snow initialization. Figure 4 indicates the difference between S1 and S2 representing increases in potential predictability by the snow initialization. Overall, more than 10% (0.1) increases in potential predictability are found over large areas of the Eurasian and North American continents. The predictability increase is highest in the earliest period of hindcast (days 1–15) and decreases with time. Even so, considerable gains exist even at more than 1-month lead, especially over the central and eastern part of the Eurasian continent, northwestern parts of United States and Canada, and the Tibetan Plateau. Large gains beyond 15 days ahead are mostly confined to the midlatitudes. Relatively small or even negative changes are found in northernmost and western Eurasia. It is notable that the degree and spatial pattern of potential predictability improvement is dependent on the season: potential predictability improvements become larger in the later part of cold season. This is likely related to the seasonal cycle of snow depth and associated meridional march of the snow line, which gives drastic differences in local climate sensitivity to imposed snow anomalies. This tendency, large gains in

the midlatitudes in the later part of cold season, is very consistent with Overland et al.'s (2011) finding; during snowmelt season, snow–atmosphere coupling is strongest over many parts of midlatitude Eurasia and America. These are further discussed in the following sections.

From the definition of the r^2 metric, we may presume that the potential predictability improvement is attributed to forced external signals invoked by the initialized snow depth. We check this with the signal-to-noise ratio (SNR), the ratio of the variance that is generated externally by given forcings or boundary conditions (snow depth in this study) to the variance that is generated internally by the chaotic atmosphere. Following Rowell (1998), the total variance of ensemble simulation (σ^2_{tot}) can be decomposed into the external (signal; σ^2_{ext}) and internal (noise; σ^2_{int}) variances. The quantities σ^2_{ext} and σ^2_{int} are expressed as

$$\sigma^2_{\text{ext}} = \sigma^2_{\text{ensm}} - \frac{1}{n}\sigma^2_{\text{int}} \quad \text{and}$$

$$\sigma^2_{\text{int}} = \frac{1}{N(n-1)} \sum_{i=1}^{N} \sum_{j=1}^{n} (x_{ij} - \overline{x}_i)^2 \quad \text{and}$$

$$\sigma^2_{\text{ensm}} = \frac{1}{N-1} \sum_{i=1}^{N} (\overline{x}_i - \overline{\overline{x}})^2$$

where i is the number of ensemble hindcasts performed; j is the number of ensemble member ($n = 16$); $\overline{x}_i$ is the ensemble mean; and $\overline{\overline{x}}$ is the climatological mean. The SNR of the modeling system is defined as the ratio between σ^2_{ext} and σ^2_{int}.

Figure 5 shows the difference in SNR between S1 and S2 series. The spatial pattern and seasonality of SNR increase are almost same to those of the r^2 increase. This indicates that the initialized snow depth provides forced variance in the model hindcasts, which contributes to the potential predictability increase.

Despite overall increase in r^2 values and SNR, it should be noted that those only represent idealized potential increase in the predictability skill, which is not directly linked with a practical increase in prediction skill. Increases in r^2 values and SNR could only result from higher agreement in prescribed initial land surface conditions used for S1 series since the unperturbed, identical snow condition was used throughout 16 ensemble members. The practical predictability gain with respect to the observation is examined in section 3d.

b. *Snow–albedo feedback strength and predictability gains*

Presumably, the impacts of snow initialization on simulated SAT can mainly be attributed to the changes in surface albedo and the resulting change in absorption of incoming solar radiation. For instance, a positive anomaly of snow depth and snow cover can lead to more reflection of incoming solar radiation that will decrease surface air temperature, which, in turn, will sustain snow depth and cover anomaly. Repetitions of this cycle tend to lead a positive feedback between snow and temperature, the so-called snow–albedo feedback. According to Cess and Potter (1988) and Qu and Hall (2006), the strength of snow–albedo feedback can be quantified as

$$\frac{\partial Q_{\text{net}}}{\partial T_s} = -Q \frac{\partial \alpha_p}{\partial \alpha_s} \frac{\Delta \alpha_s}{\Delta T_s}.$$

Here, Q and Q_{net} are incoming and net shortwave radiation at the top of atmosphere, α_p and α_s are planetary and surface albedo, and T_s is surface air temperature. The Q can be assumed to be a constant and the coefficient $\partial\alpha_p/\partial\alpha_S$ mainly depends on the average transmissivity of the clear-sky atmosphere, not directly associated with snow. Therefore we may regard the factor $\Delta\alpha_S/\Delta T_S$ as an indicator of the snow–albedo feedback strength (SAF). This term can be further decomposed into the product of two sensitivity terms as

$$\frac{\Delta \alpha_s}{\Delta T_s} = \frac{\Delta \alpha_s}{\Delta \text{SC}} \frac{\Delta \text{SC}}{\Delta T_s},$$

where SC indicates snow cover and T_s indicates surface air temperature.

We estimate the two terms, the sensitivity of surface albedo to snow cover and the sensitivity of snow cover to surface air temperature, from the linear regression analysis between the two variables. Monthly anomalies of surface albedo, snow cover, and SAT from the S1 experiments are utilized. Note that the results from the S2 experiments are similar to those of S1. Figure 6 shows calculated SAF for the late winter and fall. Strong SAF is mainly found over the midlatitudes between 30° and 50°N in both continents while SAF is relatively weak over higher latitudes. When comparing fall and late winter, SAF shows a notable difference. Strong SAF is found over larger areas in the middle to high latitudes in late winter compared to fall. High SAF agrees well with large predictability gains seen in Fig. 4, regarding both regions and seasonality, which indicates a dominant influence of the snow–albedo feedback on predictability gains.

Of the two terms included in SAF, the first term ($\Delta\alpha_S/\Delta$SC), the sensitivity of surface albedo to snow cover, remains more or less constant for the two periods. This means the intrinsic sensitivity of surface albedo to snow cover change has little variation during the cold

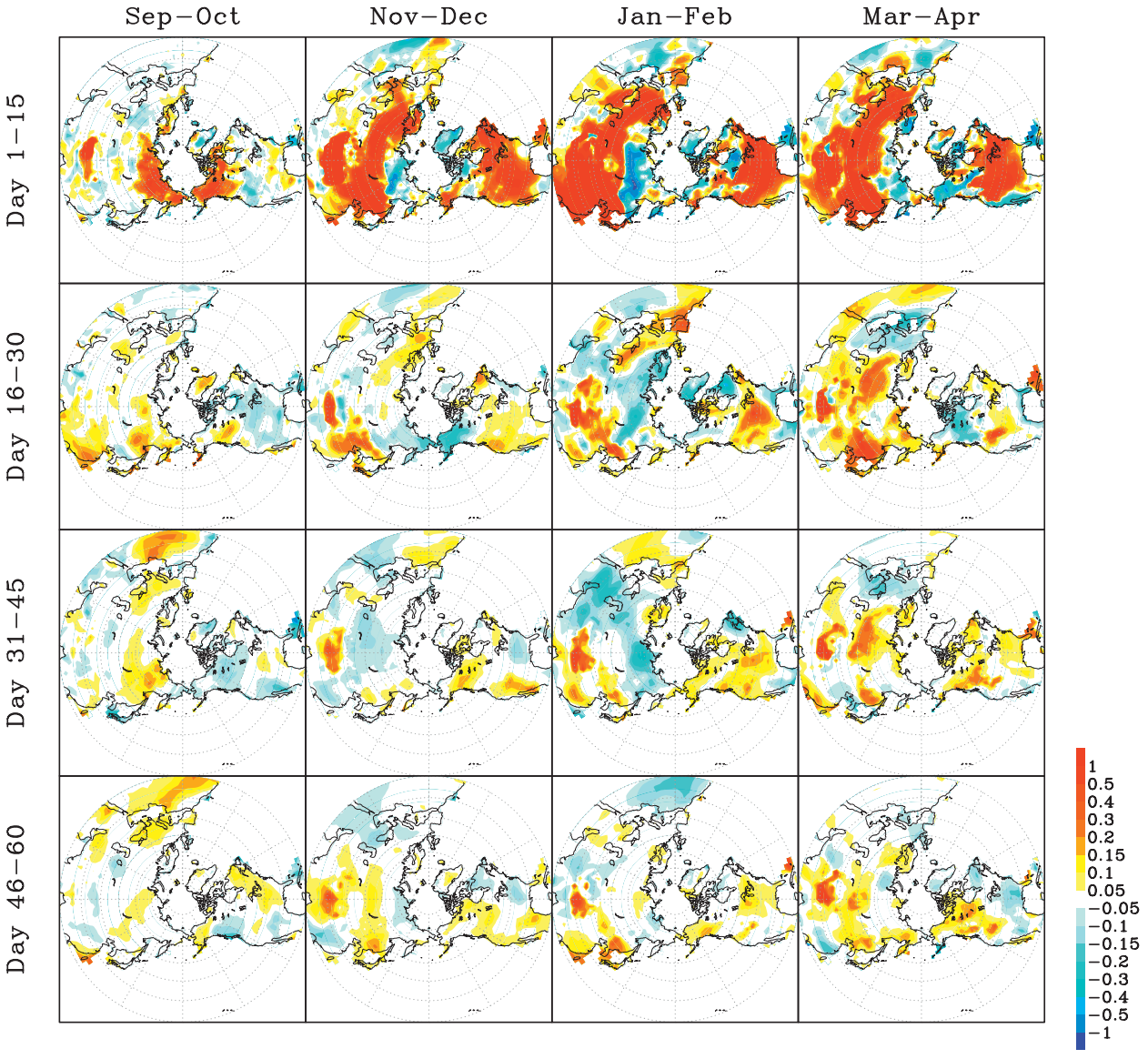

FIG. 5. As in Fig. 4, but for signal-to-noise ratio.

season. Vegetation and soil characteristics may affect this term also, but they also have little variation during the cold season. On the contrary, the second term ($\Delta SC/\Delta T_s$), the sensitivity of snow cover to SAT, shows large difference between the two periods, showing larger sensitivity in the late winter. The spatial pattern and seasonality of SAF in Figs. 6a,b is mostly contributed by this term. In high latitudes, in particular, this sensitivity is relatively low. This is because the very low air temperature prevailing during the cold period does not permit a phase change of snow. In addition, a large amount of snow has already accumulated in these regions, particularly in the later period of cold season, which leads to relatively less sensitivity of snow cover changes to imposed SAT anomalies. This is further analyzed in the next section in association with the snow depth–snow cover sensitivity. In the midlatitudes a clear seasonal dependency is found in the sensitivity of snow cover to SAT with slightly stronger sensitivity in the late winter compared to autumn. This can be due to the seasonal difference in the direction of the marching snow line (representing the 15% snow cover fraction in Fig. 2). From fall to early winter, the snow line gradually moves southward from high latitudes to midlatitudes. In other words, local snow anomalies over the midlatitudes are largely determined by the amount of new accumulation of snowfall, rather than by preexisting snow anomalies. In late winter to spring, on the contrary, snowpack

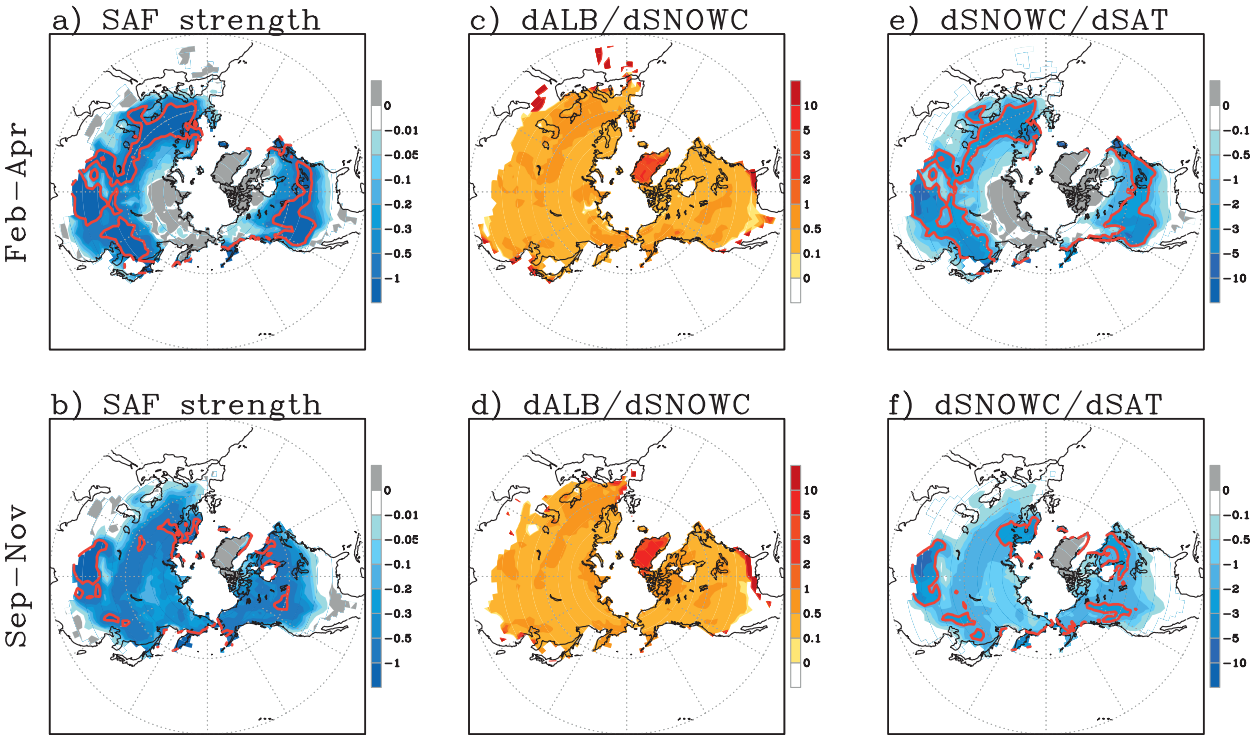

FIG. 6. (a),(b) Snow–albedo feedback strength ($\Delta\alpha_s/\Delta$SAT) in the S1 experiments. Red contour lines indicate -1% K^{-1} for comparison. (c),(d) Sensitivity of surface albedo to snow cover ($\Delta\alpha_s/\Delta$SC). (e),(f) Sensitivity of snow cover to SAT (ΔSC/ΔSAT). Red contour lines indicate -2 K^{-1} for comparison: (top) Feb–Apr and (bottom) Sep–Nov.

is disappearing from midlatitudes and snow line retreats toward north, presumably with relatively less new snow accumulation. This means that local snow anomalies are more determined by preexisting snow anomalies. Therefore, existing snow anomalies more directly lead to prolonged or shortened snow cover, and consequently lead to higher SAF in the late winter. Additionally, latent heat changes during and after snowmelt give additional impacts on SAT, which can extend the memory of winter snow mass into spring as suggested by Yeh et al. (1983).

c. *Sensitivity of snow cover to snow depth change*

In CAM3, the fractional snow cover is necessary for calculating the surface albedo. Therefore, the snow cover is estimated from snow depth following a simple empirical relationship,

$$\mathrm{SC} = D/(10 \times \mathrm{zlnd} + D),$$

where SC is snow cover (fraction), D is snow depth (m), and zlnd is the momentum roughness length for soil (0.01 m by default). Figure 7b represents this relationship between snow cover and depth in the model simulation. Here, it is clearly seen that a little (large) change in snow depth could result in a large (little) change in snow cover if there is little (large) amount of preexisting snow. Therefore, we can expect that, with same snow depth anomalies, the relatively shallow snow at middle latitudes will make a bigger change in snow cover fraction. Therefore, this sensitivity is dependent on the seasonality and spatial variation of background snow depths and therefore affects SAF as we initialize snow depth in the model.

Figure 7a indicates the sensitivity of monthly snow cover to snow depth anomalies estimated from the S1 experiment through the linear regression analysis. As expected, high sensitivity is found over midlatitudes in both Eurasia and North America, but the sensitivity is very low over the high latitudes, where mean snow depths are relatively high. Note that the sensitivity is low also over the southwestern part of Tibetan Plateau, where background snow depth is high because of high altitude. Overall, regions of high sensitivity match well with regions of high predictability increases from snow depth initialization. This means that over high-latitude regions, where the background snow depth is high, initialized snow depth anomalies may lead to smaller changes in snow cover compared to the midlatitudes. This can directly affect the SAF and predictability gains, their seasonality, and spatial variation. A scatter

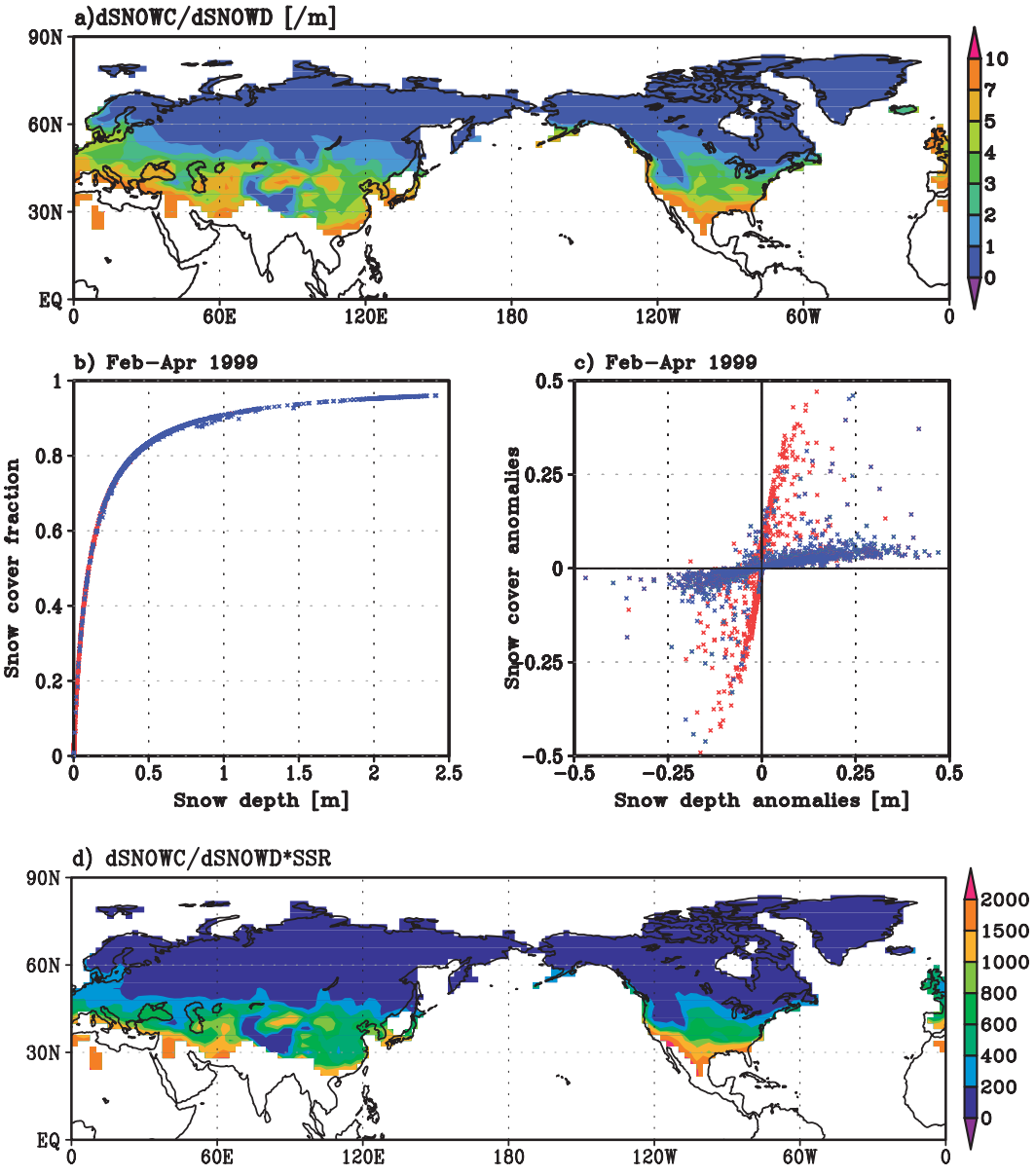

FIG. 7. (a) Sensitivity of snow cover to snow depth changes (ΔSC/ΔSD) estimated from the S1 experiments for February–April. Scatterplots of (b) snow depth vs snow cover fraction and (c) snow depth anomalies vs snow cover anomalies. (d) ΔSC/ΔSD multiplied with incident shortwave radiation at surface (SSR).

diagram of snow cover anomalies versus snow depth anomalies during a specific period (Fig. 7c) shows a clear contrast between low sensitivity in the high latitudes (60°–90°N; blue dots) and high sensitivity in the mid-latitudes (30°–50°N; red dots). It is notable that the change from low sensitivity regime to high sensitivity regime seems to happen abruptly. Therefore, this sensitivity could contribute strongly to a clear distinction between high and low SAF region. In addition, a sharp latitudinal difference in incoming solar radiation in the winter Northern Hemisphere reinforces the distinction of high and low SAF with latitude. In boreal winter, incoming solar radiation over the high-latitude regions is extremely low (e.g., polar night). Therefore, even with large snow depth or fraction anomalies, snow–albedo feedback is very weak. Figure 7d indicates the sensitivity of monthly snow cover to snow depth anomalies multiplied with incoming shortwave radiation at the surface. This approximates the snow depth to albedo effect at surface energy balance and more clearly highlights the

region of strong snow–atmosphere coupling over midlatitudes in this period.

d. Predictability increases conditional to sign of initial snow depth anomalies

One notable feature found in the impacts of snow initialization is a large asymmetry in the degree of predictability increase with respect to the sign of initial snow depth anomalies. The potential predictability gains from hindcasts started with above- and below-normal snow depth anomalies are compared in Fig. 8. Across all lead times, predictability increases are larger for hindcasts starting with positive snow depth anomalies compared to those with negative anomalies. This tendency is distinct in the midlatitude regions where largest predictability increases from snow depth initialization exist. This asymmetry can be explained by the possible dependence of snow depth memory on the sign of its anomalies. If snowpack melts over a large area under large-scale warming in the atmosphere, a snowpack with negative depth anomalies will be more quickly melted away compared to a snowpack with positive depth anomalies. Snow–albedo feedback [less snow cover leads to more absorption of shortwave radiation (SW) and warming] may accelerate snow melting and thus the snowpack loses its memory more quickly. On the contrary, a snowpack with positive depth anomalies persists longer by attenuating the initial warming signal through a negative feedback, which may provide the modeling system with a longer memory and higher predictability increases.

e. Gains in practical predictability with respect to observation

Finally, we estimate the practical predictability gain from snow initialization by comparing hindcasts with observations. Practical predictability for each experiment series is also quantified by the *r*-square metric (r^{*2}). Here, r^* indicates ordinary correlation coefficients between the ensemble mean hindcasts and the SAT observations. Before calculating r^{*2}, negative correlations were set to 0 by assuming that they reflects sampling noise by following Koster et al. (2010b). This inhibits spurious predictability gains to be rewarded from large negative correlation in the simulation (e.g., a change from -0.3 to 0.2 of r^* would get too much gains but is of no practical value). Figure 9 shows difference of r^{*2} between the S1 and S2 experiment sets. Daily 2-m air temperature from NCEP–NCAR reanalysis II is used as an alternative to observations. Significance levels of the differences are determined by a Monte Carlo approach. At a given location, for a given lead, r^{*2} difference is calculated repeatedly by reshuffling the observation time series (i.e., generating random permutations of original time series). For each period and lead, 10 000 iterations are performed, and differences at targeted confidence limits (upper and lower 1%) are determined.

Although most of potential gains found in Fig. 4 disappear or are reduced, positive contributions to predictability are still found over some mid- to high-latitude regions. Many features are consistent with the potential predictability gains in Fig. 4. The increase in prediction skill is modest in early fall but a considerable increase in skill is found in the rest of the cold season, particularly over East Asia, central and northeastern Eurasia, and northwestern America. Again, increases in skill are minimal in the high latitudes, where the SAF in the model is shown to be weak. A distinct difference from the potential predictability increases is that their large gains in the day-1–15 hindcasts almost disappear in the practical predictability estimates. This is thought to be because the impacts of atmospheric initial conditions dominate the predictability increases from snow initialization on relatively short (less than 2 weeks) timescale hindcasts. Although the large potential predictability increases found over western Russia, Eastern Europe, the Tibetan Plateau, and northern North America mostly vanished in the practical predictability estimates, there are consistent skill increases across different lead times in some specific regions, like East Asia, central Eurasia, and North America. This suggests a useful contribution of snow initialization may exist even beyond the subseasonal time scale. However, over some places in the middle to high latitudes, snow initialization rather lowers hindcast skill (negative gains). Uncertainties arisen from used snow data, model's parameterization, and initialization method might contribute to this negative impact. This is further discussed in the next section.

4. Summary and discussion

In the present study, a number of retrospective ensemble hindcasts of the CAM3 were performed with and without snow initialization for 12 cold seasons (1989–2010) in order to investigate the impacts of snow initialization on the subseasonal to seasonal prediction of air temperature. The CMC daily snow depth analysis was used to define initial snow states with an anomaly rescaling method to account for model's bias compared to observed snow. The results show that a considerable increase in potential predictability can be achieved by snow initialization, especially in the midlatitudes in late winter and early spring, where the strength of surface albedo feedback is strong. East Asia, central Eurasia, and western North America are key regions where

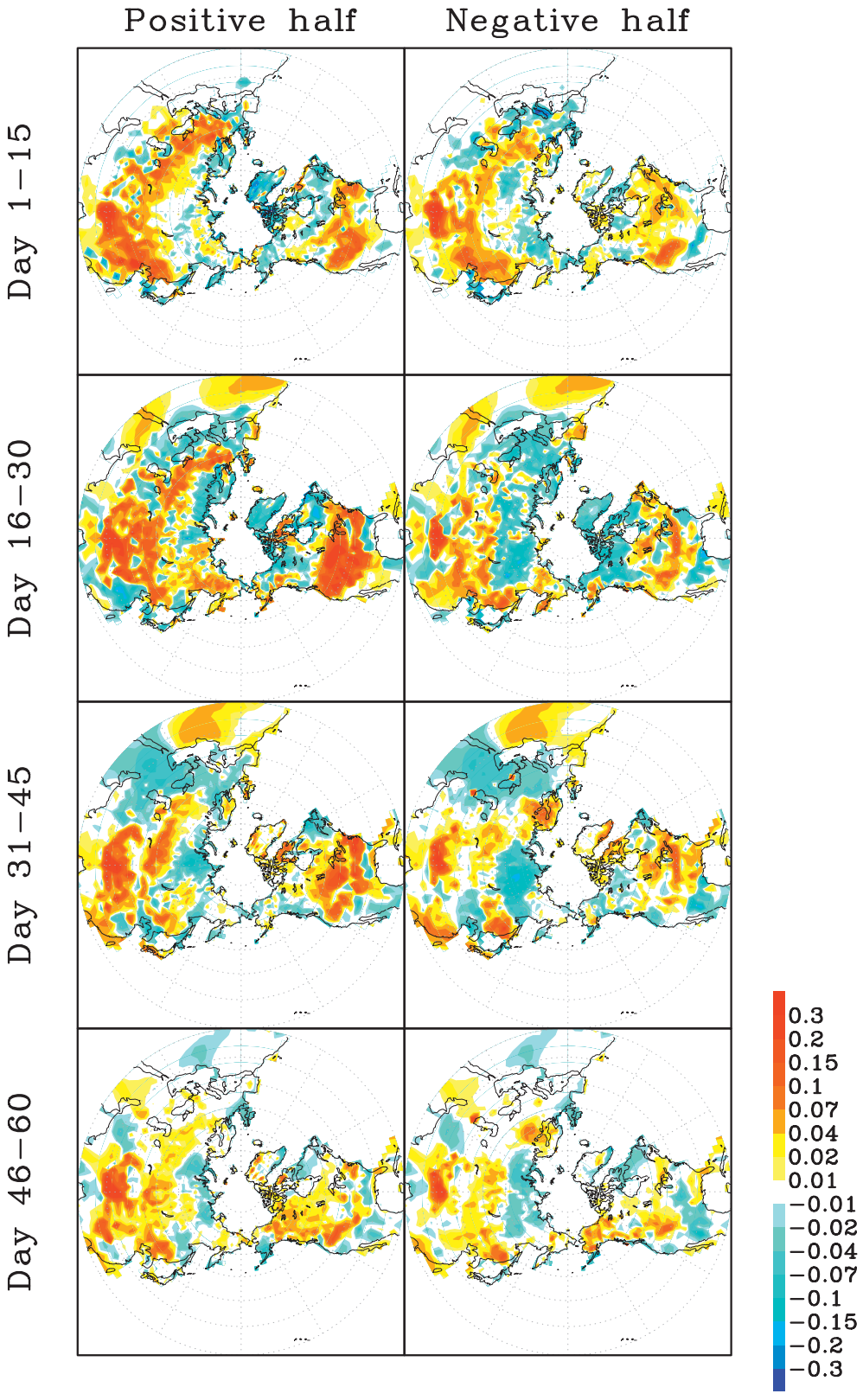

FIG. 8. Change in potential predictability (r^2) of SAT using the snow depth initialization (S1 − S2) in hindcasts starting February–April initialized with (left) positive and (right) negative snow depth anomalies: (top to bottom) day 1–15 to 46–60.

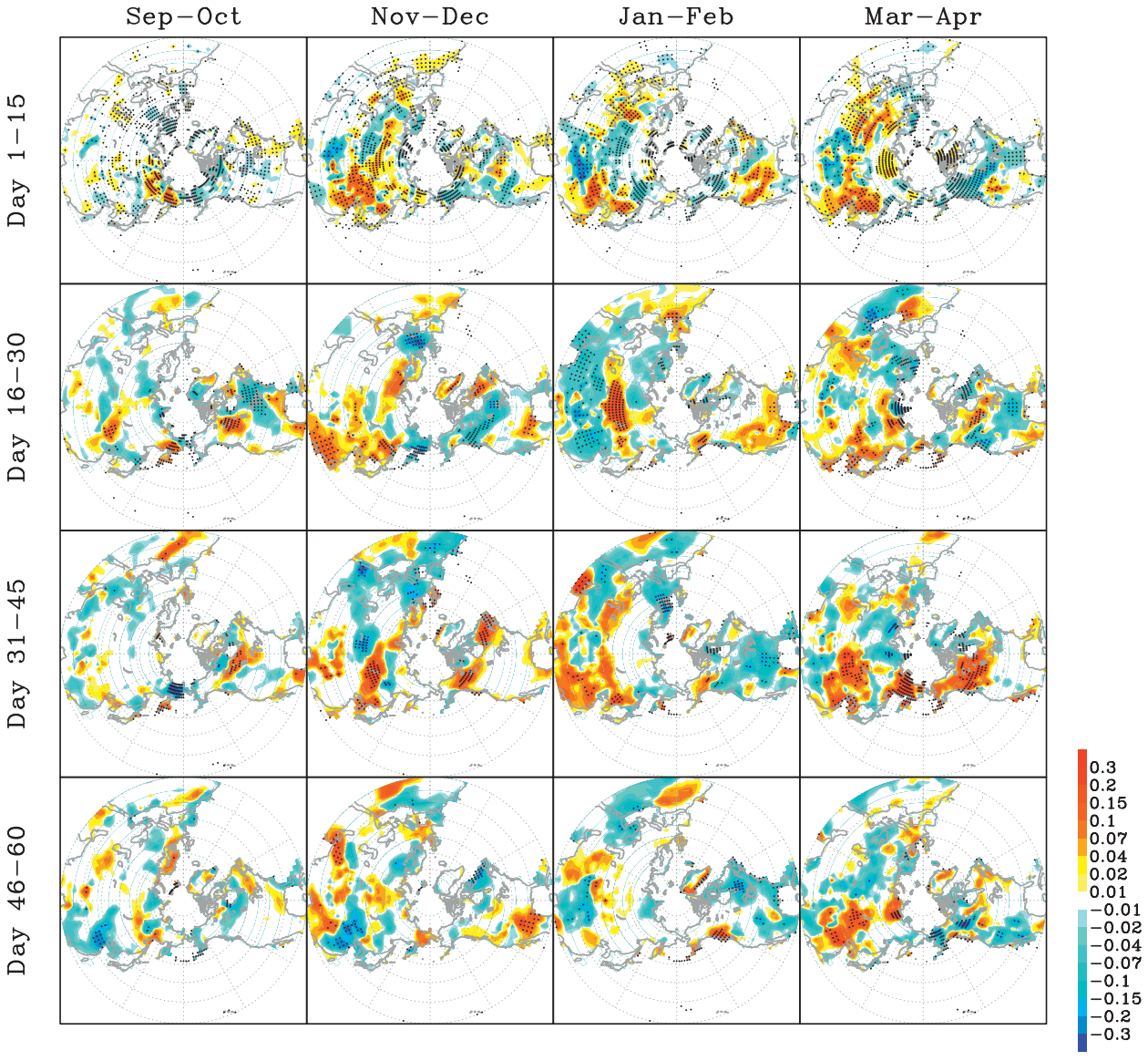

FIG. 9. Change in SAT forecast skill (r^{*2} values from ensemble mean forecasts and observations) using snow depth initialization (S1 − S2). Dots indicate regions where the change is statistically significant at the 99% confidence level, which is determined by a Monte Carlo approach (see details in the section 3e): (left to right) Sep–Oct to Mar–Apr and (top to bottom) day 1–15 to 46–60.

potential predictability increases are relatively well related to practical predictability increase.

There are some important caveats to bear in mind when interpreting the results of this study. First, the initialized snow states in these preliminary experiments, which are replaced rather than assimilated, are not physically balanced with initial atmospheric conditions as well as other land surface conditions. This may lead to little increases in practical predictability in short-term (1–15 days) hindcasts (Fig. 9), although large increases are obtained in potential predictability (Fig. 4). Because snow states are physically linked with other land surface properties like soil temperature and moisture, these need to be balanced with initialized snow depth. An appropriate assimilation system may further enhance the predictability increases. Second, predictability increases are relatively small over high-latitude regions near the Atlantic and Arctic Ocean like Western Europe, Scandinavia, and eastern North America. This may be due to the limitation of using an atmospheric only GCM. Despite its likely considerable importance for regional climate over the Arctic and extratropics, the impacts of Arctic sea ice variations are not included in the experiments. Moreover, the anomaly persistence

method for prescribing SSTs might be a reasonable method for tropical SST anomalies but is very likely to have negative effect on climate simulations over the Atlantic basin where air–sea interaction is very strong on shorter time scales than in the tropics. Third, the present study considers only the local impacts of initialized snow through local feedback process. However, large-scale snow condition may excite planetary waves perturbing the large-scale atmospheric circulations, which may well exert remote impacts (Cohen et al. 2009; Saito et al. 2001). As recently suggested by Smith et al. (2011) and Brands et al. (2012), the atmospheric circulation responses to the imposed snow anomalies and their impacts on predictability are key features of the impact of snow on seasonal climate that need further investigation. Fourth, present study focuses on the SAF in interpreting the impacts of snow on potential predictability. Even though the SAF is a major factor determining snow–atmosphere interaction, thermal insulation and hydrological effect from snow are known to have significant impacts on surface climate. According to recent model studies, the thermal insulation effect of snow cover strongly affects heat fluxes between soil and atmosphere (Woo et al. 2012). This can be a slower process compared to the SAF process, which can have significant effect during and after snow melting period. Hydrological change through soil moisture also has an important indirect effect on evaporation and energy fluxes after snow melting (Brands et al. 2012; Overland et al. 2011), which may have a secondary impact on precipitation as well as temperature. Therefore, these factors should be considered particularly for assessing predictability gains in association with snow melting. Fifth, although meaningful gains in SAT predictability can be achieved by initialized snow depth, this can be model dependent as it is widely known that climate models still have large biases and intermodel spread in the high latitudes and Arctic. Simulated SAF and associated impacts of snow initialization can be sensitive to model bias. Therefore, model deficiencies in the snow parameterization need to be considered to interpret results. The representation of the snow cover fraction has a significant influence in determining surface albedo and thus on the surface radiation balance, but it varies greatly with parameterization method (Kim et al. 1996). This could be a source of large uncertainty. This study was based on a relatively old version of CAM with a relatively simple parameterization of snow fraction based on the snow depth. Therefore, we plan to use an updated CAM with an improved parameterization of snow cover fraction that considers the snow compact and snow density variation (Kim 2002). In addition to the model's deficiency, the limitation of the snow data should be considered. Apart from the quality of used snow data, relatively short availability (12 yr) of snow data limits statistical robustness of the results. We plan to reassess this with an extended hindcast experiment of the updated CAM with an idealized snow data either from reanalysis or from long-term simulation of model.

Despite limitations, overall results in the present study clearly demonstrate the usefulness of snow depth information to improve the predictability of subseasonal prediction. This emphasizes the importance of accurate snow data and improvements in snow parameterization.

Acknowledgments. This work was funded by the Korea Meteorological Administration Research and Development Program under Grant CATER 2012-3061 (PN12010). Seong-Joong Kim was supported by the project "Reconstruction and Observation of Components for the Southern and Northern Annular Mode to Investigate the Cause of Polar Climate Change" (PE12010) of Korea Polar Research Institute. This work was partly supported by Swedish International Development Cooperation Agency SIDA (Project SWE-2009-245). Chris Folland was supported by the Joint DECC/Defra Met Office Hadley Centre Climate Programme (GA01101). The paper contributes to the Swedish strategic research area Modeling the Regional and Global Earth System (MERGE). We thank three anonymous reviewers for insightful comments and suggestions.

REFERENCES

Alexander, M. A., U. S. Bhatt, J. E. Walsh, M. S. Timlin, J. S. Miller, and J. D. Scott, 2004: The atmospheric response to realistic Arctic sea ice anomalies in an AGCM during winter. *J. Climate,* **17,** 890–905.

Ambaum, M. H. P., and B. J. Hoskins, 2002: The NAO troposphere–stratosphere connection. *J. Climate,* **15,** 1969–1978.

Armstrong, R., 2001: Historical Soviet daily snow depth version 2 (HSDSD). National Snow and Ice Data Center, Boulder, CO, CD-ROM.

Baldwin, M. P., D. B. Stephenson, D. W. J. Thompson, T. J. Dunkerton, A. J. Charlton, and A. O'Neill, 2003: Stratospheric memory and skill of extended-range weather forecasts. *Science,* **301,** 636–640.

Brands, S., R. Manzanas, J. M. Gutiérrez, and J. Cohen, 2012: Seasonal predictability of wintertime precipitation in Europe using the snow advance index. *J. Climate,* **25,** 4023–4028.

Brasnett, B., 1999: A global analysis of snow depth for numerical weather prediction. *J. Appl. Meteor.,* **38,** 726–740.

Brown, R. D., and B. Bruce, 2010: Canadian Meteorological Centre (CMC) daily snow depth analysis data. National Snow and Ice Data Center Boulder, CO, digital media. [Available online at http://nsidc.org/data/nsidc-0447.html.]

——, B. Brasnett, and D. Robinson, 2003: Gridded North American monthly snow depth and snow water equivalent for GCM evaluation. *Atmos.–Ocean,* **41,** 1–14.

Cess, R. D., and G. L. Potter, 1988: A methodology for understanding and intercomparing atmospheric climate feedback processes in general circulation models. *J. Geophys. Res.,* **93** (D7), 8305–8314.

Cohen, J., and D. Rind, 1991: The effect of snow cover on the climate. *J. Climate,* **4,** 689–706.

——, and C. Fletcher, 2007: Improved skill of Northern Hemisphere winter surface temperature predictions based on land–atmosphere fall anomalies. *J. Climate,* **20,** 4118–4132.

——, and J. Jones, 2011: A new index for more accurate winter predictions. *Geophys. Res. Lett.,* **38,** L21701, doi:10.1029/2011GL049626.

——, M. Barlow, P. J. Kushner, and K. Saito, 2007: Stratosphere–troposphere coupling and links with Eurasian land surface variability. *J. Climate,* **20,** 5335–5343.

——, ——, and K. Saito, 2009: Decadal fluctuations in planetary wave forcing modulate global warming in late boreal winter. *J. Climate,* **22,** 4418–4426.

Collins, W. D., and Coauthors, 2004: Description of the NCAR Community Atmosphere Model (CAM 3.0). National Center for Atmospheric Research Tech. Note NCAR/TN–464+STR, 226 pp.

Dee, D. P., and S. Uppala, 2009: Variational bias correction of satellite radiance data in the ERA-Interim reanalysis. *Quart. J. Roy. Meteor. Soc.,* **135,** 1830–1841.

——, and Coauthors, 2011: The ERA-Interim reanalysis: Configuration and performance of the data assimilation system. *Quart. J. Roy. Meteor. Soc.,* **137,** 553–597.

Deser, C., G. Magnusdottir, R. Saravanan, and A. Phillips, 2004: The effects of North Atlantic SST and sea ice anomalies on the winter circulation in CCM3. Part II: Direct and indirect components of the response. *J. Climate,* **17,** 877–889.

——, R. A. Tomas, and S. Peng, 2007: The transient atmospheric circulation response to North Atlantic SST and sea ice anomalies. *J. Climate,* **20,** 4751–4767.

Fletcher, C. G., S. C. Hardiman, P. J. Kushner, and J. Cohen, 2009a: The dynamical response to snow cover perturbations in a large ensemble of atmospheric GCM integrations. *J. Climate,* **22,** 1208–1222.

——, P. J. Kushner, A. Hall, and X. Qu, 2009b: Circulation responses to snow albedo feedback in climate change. *Geophys. Res. Lett.,* **36,** L09702, doi:10.1029/2009GL038011.

Folland, C., A. A. Scaife, J. Lindesay, and D. B. Stephenson, 2011: How potentially predictable is northern European winter climate a season ahead? *Int. J. Climatol.,* **32,** 801–818.

Ge, Y., and G. Gong, 2008: Observed inconsistencies between snow extent and snow depth variability at regional/continental scales. *J. Climate,* **21,** 1066–1082.

Hardiman, S. C., P. J. Kushner, and J. Cohen, 2008: Investigating the ability of general circulation models to capture the effects of Eurasian snow cover on winter climate. *J. Geophys. Res.,* **113,** D21123, doi:10.1029/2008JD010623.

Honda, M., J. Inoue, and S. Yamane, 2009: Influence of low Arctic sea-ice minima on anomalously cold Eurasian winters. *Geophys. Res. Lett.,* **36,** L08707, doi:10.1029/2008GL037079.

Ineson, S., and A. A. Scaife, 2009: The role of the stratosphere in the European climate response to El Niño. *Nat. Geosci.,* **2,** 32–36.

——, ——, J. R. Knight, J. C. Manners, N. J. Dunstone, L. J. Gray, and J. D. Haigh, 2011: Solar forcing of winter climate variability in the Northern Hemisphere. *Nat. Geosci.,* **4,** 753–757.

Jeong, J.-H., C.-H. Ho, D. L. Chen, and T.-W. Park, 2008: Land surface initialization using an offline CLM3 simulation with the GSWP-2 forcing dataset and its impact on CAM3 simulations of the boreal summer climate. *J. Hydrometeor.,* **9,** 1231–1248.

——, T. Ou, H. W. Linderholm, B.-M. Kim, S.-J. Kim, J.-S. Kug, and D. Chen, 2011: Recent recovery of the Siberian high intensity. *J. Geophys. Res.,* **116,** D23102, doi:10.1029/2011JD015904.

Kanamitsu, M., W. Ebisuzaki, J. Woollen, S.-K. Yang, J. J. Hnilo, M. Fiorino, and G. L. Potter, 2002: NCEP–DOE AMIP-II Reanalysis (R-2). *Bull. Amer. Meteor. Soc.,* **83,** 1631–1643.

Kim, K.-Y., 2002: Investigation of ENSO variability using cyclostationary EOFs of observational data. *Meteor. Atmos. Phys.,* **81,** 149–168.

——, G. R. North, and J. Huang, 1996: EOFs of one-dimensional cyclostationary time series: Computations, examples, and stochastic modeling. *J. Atmos. Sci.,* **53,** 1007–1017.

Koster, R. D., and Coauthors, 2004: Realistic initialization of land surface states: Impacts on subseasonal forecast skill. *J. Hydrometeor.,* **5,** 1049–1063.

——, S. P. P. Mahanama, B. Livneh, D. P. Lettenmaier, and R. H. Reichle, 2010a: Skill in streamflow forecasts derived from large-scale estimates of soil moisture and snow. *Nat. Geosci.,* **3,** 613–616.

——, and Coauthors, 2010b: Contribution of land surface initialization to subseasonal forecast skill: First results from a multi-model experiment. *Geophys. Res. Lett.,* **37,** L02402, doi:10.1029/2009GL041677.

——, and Coauthors, 2011: The second phase of the Global Land–Atmosphere Coupling Experiment: Soil moisture contributions to subseasonal forecast skill. *J. Hydrometeor.,* **12,** 805–822.

Kumar, A., and F. Yang, 2003: Comparative influence of snow and SST variability on extratropical climate in northern winter. *J. Climate,* **16,** 2248–2261.

——, Q. Zhang, P. Peng, and B. Jha, 2005: SST-forced atmospheric variability in an atmospheric general circulation model. *J. Climate,* **18,** 3953–3967.

Oleson, K. W., and Coauthors, 2004: Technical description of the Community Land Model (CLM). National Center for Atmospheric Research Tech. Note NCAR/TN-461+STR, 186 pp.

Orsolini, Y. J., and N. G. Kvamstø, 2009: Role of Eurasian snow cover in wintertime circulation: Decadal simulations forced with satellite observations. *J. Geophys. Res.,* **114,** D19108, doi:10.1029/2009JD012253.

Overland, J. E., K. R. Wood, and M. Wang, 2011: Warm Arctic—Cold continents: Climate impacts of the newly open Arctic Sea. *Polar Res.,* **30,** 15787, doi:10.3402/polar.v30i0.15787.

Peings, Y., H. Douville, R. Alkama, and B. Decharme, 2010: Snow contribution to springtime atmospheric predictability over the second half of the twentieth century. *Climate Dyn.,* **37,** 985–1004.

Qu, X., and A. Hall, 2006: Assessing snow albedo feedback in simulated climate change. *J. Climate,* **19,** 2617–2630.

Rayner, N. A., and Coauthors, 2003: Global analyses of sea surface temperature, sea ice, and night marine air temperature since the late nineteenth century. *J. Geophys. Res.,* **108,** 4407, doi:10.1029/2002JD002670.

Reynolds, R. W., N. A. Rayner, T. M. Smith, D. C. Stokes, and W. Wang, 2002: An improved in situ and satellite SST analysis for climate. *J. Climate,* **15,** 1609–1625.

Robinson, D. A., K. F. Dewey, and R. R. Heim, 1993: Global snow cover monitoring: An update. *Bull. Amer. Meteor. Soc.,* **74,** 1689–1696.

Rowell, D. P., 1998: Assessing potential seasonal predictability with an ensemble of multidecadal GCM simulations. *J. Climate,* **11,** 109–120.

Saito, K., J. Cohen, and D. Entekhabi, 2001: Evolution of atmospheric response to early-season Eurasian snow cover anomalies. *Mon. Wea. Rev.,* **129,** 2746–2760.

Saunders, M. A., B. Qian, and B. Lloyd-Hughes, 2003: Summer snow extent heralding of the winter North Atlantic Oscillation. *Geophys. Res. Lett.,* **30,** 1378, doi:10.1029/2002GL016832.

Shukla, J., and Coauthors, 2000: Dynamical seasonal prediction. *Bull. Amer. Meteor. Soc.,* **81,** 2593–2606.

Smith, K. L., P. J. Kushner, and J. Cohen, 2011: The role of linear interference in northern annular mode variability associated with Eurasian snow cover extent. *J. Climate,* **24,** 6185–6202.

Trenberth, K. E., G. W. Branstator, D. Karoly, A. Kumar, N.-C. Lau, and C. Ropelewski, 1998: Progress during TOGA in understanding and modeling global teleconnections associated with tropical sea surface temperatures. *J. Geophys. Res.,* **103** (C7), 14 291–14 324.

Vavrus, S., and D. Waliser, 2008: An improved parametrization for simulating Arctic cloud amount in the CCSM3 climate model. *J. Climate,* **21,** 5673–5687.

Wang, B., and Coauthors, 2008: Advance and prospectus of seasonal prediction: Assessment of the APCC/CliPAS 14-model ensemble retrospective seasonal prediction (1980–2004). *Climate Dyn.,* **33,** 93–117.

Winton, M., 2006a: Amplified Arctic climate change: What does surface albedo feedback have to do with it? *Geophys. Res. Lett.,* **33,** L03701, doi:10.1029/2005GL025244.

——, 2006b: Surface albedo feedback estimates for the AR4 climate models. *J. Climate,* **19,** 359–365.

Woo, S.-H., B.-M. Kim, J.-H. Jeong, S.-J. Kim, and G.-H. Lim, 2012: Decadal changes in surface air temperature variability and cold surge characteristics over northeast Asia and their relation with the Arctic Oscillation for the past three decades (1979–2011). *J. Geophys. Res.,* **117,** D18117, doi:10.1029/2011JD016929.

Yeh, T. C., R. T. Wetherald, and S. Manabe, 1983: A model study of the short-term climatic and hydrologic effects of sudden snow-cover removal. *Mon. Wea. Rev.,* **111,** 1013–1024.